Article

Autocatalytic Morphology Transformation Platform for Targeted Drug Accumulation

Dong-Bing Cheng, Dong Wang, Yu-Juan Gao, Lei Wang, Zeng-Ying Qiao, and Hao Wang

J. Am. Chem. Soc., **Just Accepted Manuscript** • DOI: 10.1021/jacs.8b13512 • Publication Date (Web): 25 Feb 2019

Autocatalytic Morphology Transformation Platform for Targeted Drug Accumulation

Dong-Bing Cheng, Dong Wang, Yu-Juan Gao, Lei Wang, Zeng-Ying Qiao*, Hao Wang*

CAS Center for Excellence in Nanoscience, CAS Key Laboratory for Biomedical Effects of Nanomaterials and Nanosafety, National Center for Nanoscience and Technology (NCNST), Center of Materials Science and Optoelectronics Engineering, University of Chinese Academy of Sciences, Beijing, 100190, China

Supporting Information

ABSTRACT: The precise and high-efficient drug delivery of nanomedicines into lesions remains a critical challenge in clinical translational research. Here, autocatalytic morphology transformation platform is presented for improving the tumor-specific accumulation of drugs by kinetic control. The in situ reorganization of prodrug from nanoparticle to *β*-sheet fibrous structures for targeted accumulation bases on nucleation-based growth kinetics. During multiple administrations, the autocatalytic morphology transformation can be realized for skipping slow nucleating process and construct the bulky nanoassembly instantaneously, which have been demonstrated to induce the cumulative effect of prodrug. Furthermore, the sustained drug release from fibrous prodrug depot in tumor site inhibits the tumor growth efficiently. The autocatalytic morphology transformation strategy *in vivo* offers a novel perspective for targeted delivery strategy by introducing chemical kinetics and shows great potential in disease theranostics.

INTRODUCTION

Innovative nanoscaled drug delivery systems show substantially potential in precision medicine and pharmaceutical industry, but it is reported that only ~0.7% of the administered dose on average can be accumulated in tumor site[1-5]. The possible major reasons for the inefficient accumulation are the complex tumor microenvironment and nonspecific recognition, which permit nanodrugs re-enter the bloodstream and accumulate into other organs[6-8].

The self-assembly is pervasive and plays a critical part in living organisms. By mimicking the natural self-assembly systems, many smart self-assembled materials have been developed. Recently, our group has reported assembly/aggregation induced retention (AIR) effect in disease sites *in vivo*, amplifying their sensitivity and specificity for disease diagnostics[9-11]. Moreover, various intracellular assembled prodrugs are reported and show efficient anti-cancer efficacy[12-14], even against drug-resistant cells[15]. However, the artificial nanoassembly is difficult to be constructed in organisms controllably due to the chemical complexity of the *in vivo* environment, which is a major challenge for in situ constructing assemblies in specific sites. Supramolecular self-assembly via nucleation-based mechanism has been reported in various systems, such as π-conjugated organic molecules[16], assemblages-forming macromolecules[17], and *β*-sheet-forming peptides [18-20]. Usually, the kinetic behavior of nucleation-based self-assembly is characterized by a lag period of slow nucleation, followed by a period of rapid growth, which indicates the nucleation is the rate-limiting process. Thus, an autocatalytic strategy can be used for constructing the bulky nanoassembly instantaneously through adding "seeds" to skip nucleating process[21-24].

By integrating autocatalytic self-assembly into AIR effect, we demonstrate an autocatalytic transformation strategy wherein preformed fibrous nanodrugs in the tumor site are served as "seed" fibrils for accelerating the drug accumulation (Scheme 1). A peptide-based prodrug with four moieties is developed, including (i) a hydrophobic chemodrug camptothecin (CPT), (ii) a hydrogen-bonding peptide LVFF as the scaffolds for the formation of *β*-sheet structured fibers, (iii) an enzyme-cleavable peptide GFLG, and (iv) a hydrophilic poly (ethylene glycol) (PEG) with targeting peptide RGD terminal. The stable as-prepared nanoparticles of CPT-LVFFGFLG-PEG-RGD (CPT-LFPR) are intravenously (i.v.) injected into tumor-bearing mice, which subsequently accumulate in the tumor site based on targeting effect. Then, in the presence of cathepsin B (CtsB), a significant lysosomal protease overexpressed in various tumor (including lung cancer, prostate cancer, and cervical cancer)[25,26], the nanoparticles reorganize into *β*-sheet fibrous structures due to the shedding of hydrophilic PEG-RGD shell. The preformed fibrils in the tumor act as the "seeds" for accelerating the transformation of following i.v. injected nanoparticles, which exhibit enhanced accumulation after multiple administrations, in situ constructing fibrous drug depot. Finally, the nanofibers enable sustained release of free drugs inside tumor cells, resulting in efficient inhibition of tumor growth.

RESULTS AND DISCUSSION

Scheme 1. Schematic illustration of enzyme-triggered morphology transformation and autocatalytic growth of nanofibers.

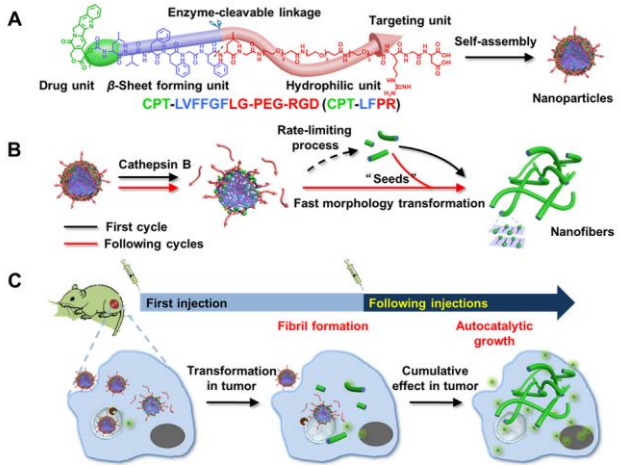

(A) Molecular structure and self-assembly behavior of CPT-LFPR. (B) The fibrils accelerate the subsequent transformation into nanofibers based on autocatalytic growth mechanism. (C) Multiple intravenous injections of nanoparticles shows the cumulative effect of fibrous prodrugs.

Enzyme-triggered morphology transformation of supramolecular prodrugs. The molecule CPT-LFPR, control groups CPT-LVFFGGGG-PEG-RGD (enzyme non-sensitive peptide, CPT-LGPR) and CPT-LVFFGF (nanofiber-forming peptide, CPT-LF) are prepared by standard solid-phase peptide synthesis and subsequent conjugation with CPT via urethane linkage (Figure S1). The structures of peptide-based prodrugs are confirmed by matrix-associated laser desorption ionization time-of-flight mass spectrometry (MALDI-TOF-MS) and ^{1}H NMR spectra (Figure S2-S8).

The responsiveness of peptide GFLG under CtsB is first confirmed by high-performance liquid chromatography (HPLC) and MALDI-TOF-MS (Figure 1A). Then the enzyme-induced morphological transformation behavior of CPT-LFPR assemblies is examined by TEM and circular dichroism (CD). In phosphate buffer solution (PB, 0.01M, pH 7.4), hydrophilic PEG-RGD is the crucial segment to stabilize the CPT-LFPR nanoassemblies as spherical structure. Transmission electron microscopy (TEM) observation shows the CPT-LFPR disperses as nanoparticles with 32.8 ± 4.3 nm (Figure 1B). Under CtsB, the morphology transition of CPT-LFPR assemblies from nanoparticles to nanofibers with the diameter of 4.5 nm is observed by TEM in 10 h. By contrary, CPT-LGPR shows no obvious change after the treatment of CtsB (Figure S9 and S10). Therefore, CPT-LFPR can be cleaved by CtsB to generate residue CPT-LF[27] (Figure S11), realizing the nanoparticles-to-nanofibers morphology change.

The driving force of transformation is first investigated by CD spectra. After incubated with CtsB for 8 h, the CPT-LFPR assemblies show a positive CD signal at 199 nm and a negative signal at 220 nm, which confirm typical β-sheet fibrous structure[10]. Nevertheless, the CPT-LFPR shows no CD signal in the absence of CtsB, suggesting

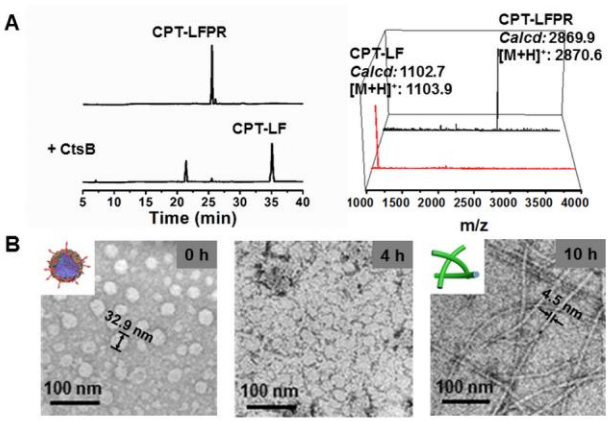

Figure 1. (A) HPLC (left) spectra of CPT-LFPR mixed with or without CtsB in acetate buffer solution (AB, 0.01M, pH 5.0) for 1 h. MOLDI-TOF (right) spectra of CPT-LFPR (black) and HPLC mobile phase at 35.1 min after the CPT-LFPR treated with CtsB (red). (B) Representative TEM images of CPT-LFPR (0.5 mg mL^{-1}) in the presence (left, PB, 0.01M, pH 7.4) of CtsB (1.0 μg mL^{-1}, AB, 0.01M, pH 5.0) in 10 h.

little β-sheet structure in spherical morphology (Figure 2A and S12). Thioflavin T (ThT, a fluorescent probe) is used to further confirm the secondary structure of the assemblies [28]. Interestingly, ThT can intercalate into the β-sheet structure and exhibit fluorescence resonance energy transfer (FRET) effect at an excitation of 375 nm with ThT as acceptor and CPT as a donor (Figure S13), which further demonstrates the nanofibers with β-sheet conformation are formed. Furthermore, the Fourier transform infrared spectroscopy (FTIR) and wide-angle X-ray scattering (WAXS) are performed to study the molecular packing mode in the β-sheet fibrous structure. The amide I region

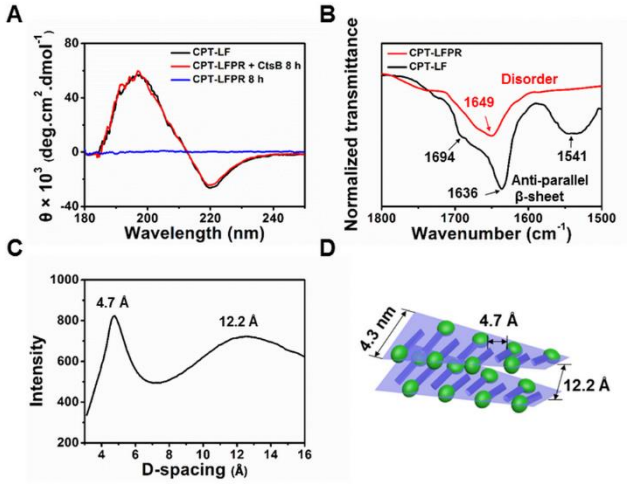

Figure 2. (A) CD spectra of CPT-LF and CPT-LFPR treated with and without CtsB in AB (0.01M, pH 5.0). (B) FTIR spectra of CPT-LFPR and CPT-LF. The peaks at 1694 cm^{-1}, 1636 cm^{-1} and 1541 cm^{-1} suggest the antiparallel β-sheet conformation. (C) Wide-angle X-ray scattering (WAXS) of CPT-LF. The *d*-spacings of 4.7 Å and 12.2 Å are attributed to the spacing of the adjacent strands and laminates, respectively. (D) Proposed antiparallel β-sheet molecular arrangement of CPT-LF.

of FTIR spectrum at 1636 cm^{-1} and 1694 cm^{-1} and amide II region peak at 1541 cm^{-1} suggest the antiparallel β-sheet conformation (Figure 2B) of CPT-LF[30]. There are two distinct peaks in WAXS, in which 4.7 Å spacing corresponds to the distance between two adjacent strands in β-sheet and 12.2 Å spacing is relevant to two sheets in the bilayers[29] (Figure 2C). According to above analysis, molecular arrangement model of nanofibers can be presented (Figure 2D), and the diameter of model nanofibers (4.3 nm) is consistent with the fibrous structure obtained from TEM (4.5 nm). Moreover, the drug release profiles are performed by dialysis method with or without CtsB. The HPLC and ^{1}H NMR spectra demonstrate the free CPT are released from CPT-LFPR in 24 h, proving that the urethane linkage can be slowly hydrolyzed[31,32] (Figure S14).

Kinetic analysis of autocatalytic morphology transformation. In order to study the autocatalytic morphology transformation, we sonicate the mature nanofibers to obtain fibrils. In the presence of fibrils, the distinct fibrous structure is observed at 4 h (Figure 3A), which is faster than that without fibrils (Figure 1B). Therefore, the fibrils can be considered as "seeds" which speed up the morphology transition from nanoparticles to nanofibers. The processes of autocatalytic growth are studied by confocal laser scanning microscopy (CLSM).[33] Under CtsB, the growth of CPT-LFPR fibers in the presence of Cy5-labeled (Figure. S15) fibrils is observed (Figure 3B). Obviously, the green nanofibers overlap with the red fibrils, which suggest the growth of CPT-LFPR nanofibers are initiated by preformed fibrils (Figure 3C).

The kinetics of autocatalytic growth are investigated by TEM and ThT fluorescence. As shown in TEM images, the length of nanofibers become longer with the addition of nanoparticles (Figure 4A and S16), and the elongation of nanofibers is proportional to the mass ratio of nanoparticles-to-fibrils, further implying that the

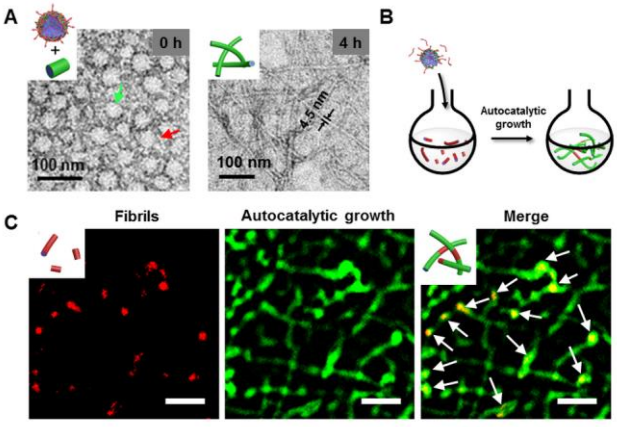

Figure 3. (A) TEM imaging of CPT-LFPR in the presence of CtsB (1.0 μg mL^{-1}) and fibrils for 4 h. Green and red arrows indicate the nanoparticles and fibrils, respectively. (B) The schematic illustration of autocatalytic morphology transformation in the presence of fibrils. (C) CLSM images of fibrils (1.0 μg mL^{-1}) and autocatalytic growth of CPT-LFPR nanofibers (0.5 mg mL^{-1}, 24 h). White arrows indicate the red fibrils. Scale bars: 2 μm.

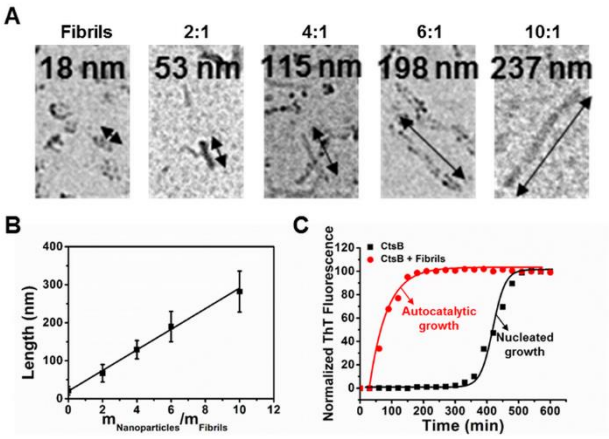

Figure 4. (A) TEM images and the corresponding length of CPT-LFPR grown from fibrils. (B) Plot showing the linear relationship of nanofiber length with $m_{nanoparticles}/m_{fibrils}$ (2:1, 4:1, 6:1 and 10:1). (C) Growth profile of CPT-LFPR nanofibers with and without fibrils monitored by ThT fluorescence in the presence of CtsB (1.0 μg mL^{-1}). Values are expressed as means ± SD (N = 3).

nanoparticles transform into fibrous structures based on the fibrils[34] (Figure 4B). The kinetics of nanofiber formation is further analyzed by ThT fluorescence to verify the autocatalytic growth process. The ThT fluorescence profile without fibrils conforms to the typical kinetic curve of nucleation-based self-assembly, showing slow nucleation (~6 h) followed by fast autocatalytic growth (~2 h) (Figure 4C). The data points can be well fitted by the Finke-Watzky (F-W) two-step model (Figure S17), which is commonly applied for reflecting the aggregation rates of nucleation-based self-assembly[35,36]. The nucleation constant k_1 and growth constant k_2 are 2.818 × 10^{-4} min^{-1} and 4.825 × 10^{-4} $min^{-1}\cdot\mu M^{-1}$, respectively. After addition of fibrils, the disappearance of lag nucleation process as well as the rapid onset of ThT fluorescence indicates the accelerated transformation from nanoparticles to nanofibers. Pseudo first order kinetic is applied for describing the autocatalytic assembly and the pseudo first-order rate constant k' is 0.017 min^{-1}, suggesting the fast growth of nanofiber in the presence of fibrils. It is speculated that the rapid autocatalytic growth of nanofibers can be applied in cell and animal level for enhancing accumulation efficiency of prodrugs.

Intracellular autocatalytic growth of nanofibers. As above-mentioned, CtsB is overexpressed in lysosome in most cancer cells, so the cellular uptake of CPT-LFPR nanoparticles and their colocalization with lysosomes in HeLa cells are monitored by CLSM. The green fluorescence of CPT become stronger with the increase of incubation time, which also can be colocalized with red fluorescence from lysosomes (stained by Lysotracker red) efficiently (Figure S18). This phenomenon suggests efficient cellular endocytosis ability and lysosomal location of CPT-LFPR[37], which meets the requirement for CtsB-triggered reorganization. The intracellular morphology transformation of CPT-LFPR is first studied by Bio-TEM (Figure 5A). After incubated with CtsB-overexpressed

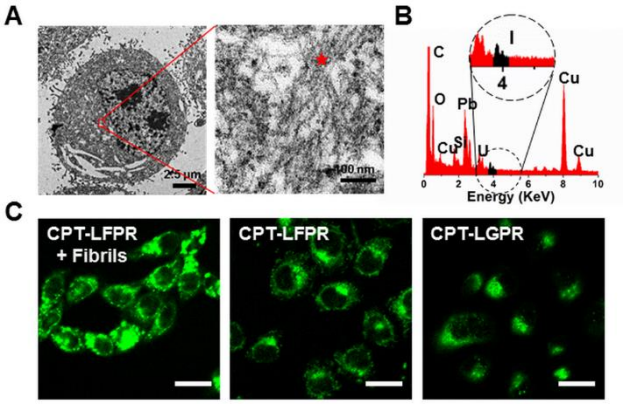

Figure 5. (A) Bio-TEM images of HeLa cells after incubation with CPT-LFPR (3 μM, 12 h). (B) The corresponding energy-dispersive profiles at the region indicated by red star in Figure 5A. (C) The intracellular CPT fluorescence monitored by CLSM for 4 h. HeLa cells are treated with or without fibrils followed by incubation with CPT-LFPR or CPT-LGPR. Scale bar: 20 μm.

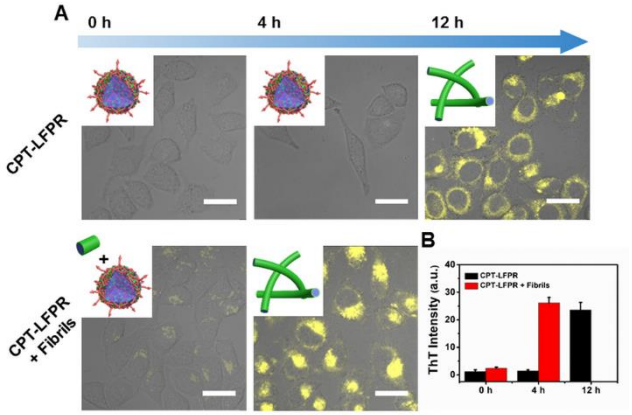

Figure 6. (A) The intracellular nanofibers monitored by ThT fluorescence in different time points. HeLa cells are treated with or without fibrils followed by incubation with CPT-LFPR (3 μM). Scale bar: 20 μm. (B) Fluorescent quantitative analysis of ThT in cells.

HeLa cells, the fibrous structures are observed in CPT-LFPR treated cells obviously, while they cannot be found in the CPT-LGPR and CPT treated cells (Figure S19). To confirm that the nanofibers originate from the transformation of CPT-LFPR nanoparticles, the element iodine is labeled onto F amino acid (Figure 5B and S20), and energy-dispersive X-ray spectroscopy (EDS) on intracellular fibrous structures reveals that iodine is detected, demonstrating the formation of CPT-LF nanofibers in cells. Flow cytometry is applied to demonstrate the intracellular retention effect of transformable CPT-LFPR (Figure S21). The Hela cells are incubated with CPT-LFPR, CPT-LGPR, and CPT for 6 h, and then the culture solutions are replaced by fresh drug-free medium. Most of the CPT fluorescence signal intensity in transformable CPT-LFPR treated cells remains up to 24 h. On the contrary, the fluorescence signal disappears quickly for CPT-LGPR and CPT treated groups. Quantitatively, the intracellular fluorescence signal of CPT-LFPR is 3-4 folds higher than that of CPT-LGPR and CPT at 24 h. Compared with the CPT-LGPR nanoparticles and free drug CPT, the higher intracellular retention of CPT-LFPR nanofibers suggests the fibrous structure exhibits slow efflux from cells. To verify the autocatalytic accumulation of prodrug in cells, the fibrils are first incubated with Hela cells, and CPT green fluorescence is observed, which demonstrates the fibrils can be internalized in cells (Figure S22). Subsequently, the cells are treated with CPT-LFPR for another 4 h, and the intracellular CPT green fluorescence is obviously stronger than the CPT-LFPR (without fibrils) and CPT-LGPR treated HeLa cells (Figure 5C), suggesting the higher cellular accumulation of CPT-LFPR in fibrils treated cells[9,12].

Interestingly, FRET effect between ThT and CPT plays a vital role in marking the intracellular CPT-LFPR nanofibers specifically, simultaneously eliminating interference from intracellular proteins with *β*-sheet structure[38]. Thus, the intracellular autocatalytic growth of nanofibers is investigated by FRET fluorescence from ThT (Ex = 405 nm, emission windows: 500-550 nm), which enhances with the formation of nanofibers. As shown in Figure 6A, the yellow ThT fluorescence confirms that the fibrils can be internalized after incubation with HeLa cells for 1 h. Subsequently, the cells are incubated with CPT-LFPR for 4 h, and the intensity of ThT fluorescence is dramatically promoted (~13 folds). By contrary, CPT-LFPR treated HeLa cells in the absence of fibrils show no fluorescence signal change in the same time scale, and the enhanced fluorescence is observed at 12 h. The fast fluorescence enhancement in fibrils treated cells can be attributed to the accelerated formation of nanofibers, which is further verified by Bio-TEM measurement (Figure S23). The TEM images show fast accumulation of nanofibers in fibrils treated cells in 4 h, while there are still nanoparticles in untreated cells. All the results prove the autocatalytic process of nanofibers in living cells, which may realize the improved anticancer capacity. The cytotoxicity of LFPR, free CPT, CPT-LGPR, and CPT-LFPR are investigated by CCK-8 assay. Figure S24 shows that CPT-LFPR (IC_{50} = 4.3 μM), close to free CPT (IC_{50} =4.1 μM), displays higher cytotoxic activity to HeLa cells than CPT-LGPR (IC_{50} =6.8 μM). Meanwhile, the free RGD peptide can compete for binding to the $\alpha_v\beta_3$ integrin on the cellular membrane and decrease the internalization of CPT-LFPR nanoparticles into the $\alpha_v\beta_3$ over-expressed HeLa cells, which result in the lower cytotoxicity. The results validate the intracellular fibrils can accelerate the transformation of CPT-LFPR from nanoparticles to nanofibers in cells, which lead to the enhanced accumulation of prodrugs and resultant highly potent inhibition ability toward tumor cells.

Targeted accumulation of prodrugs by multiple administration *in vivo*. To demonstrate the targeted accumulation of multiple administration of CPT-LFPR, the fresh Cy5-labeled CPT-LFPR and CPT-LGPR nanoparticles (Figure S25) are i.v. injected into mice at day 1 and day 4. As shown in Figure 7A, the real-time fluorescence of CPT-LFPR in tumor at day 4 and 6 is stronger than that at day 1 and day 3, respectively. In contrast, for CPT-LGPR, there is no obvious fluorescent change between the two injections.

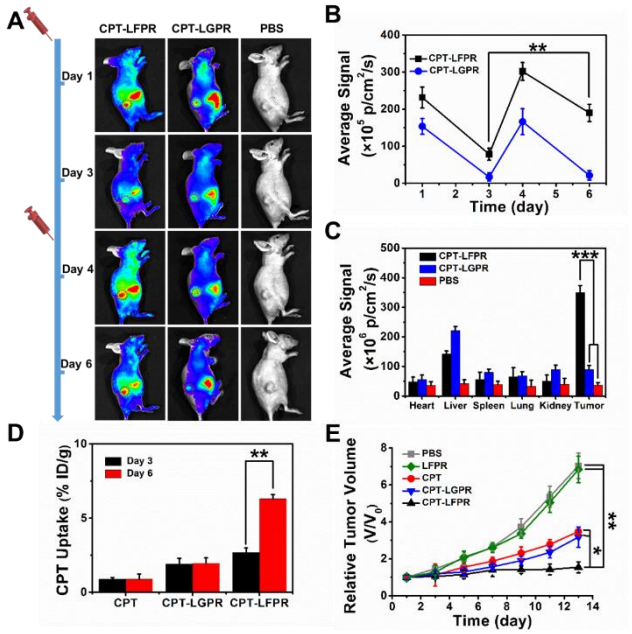

Figure 7. (A) *In vivo* fluorescence images of tumor-bearing mice after i.v. injection of CPT-LFPR, CPT-LGPR, and PBS at day 1 and day 4. Red circles indicate the tumors. (B) Fluorescent quantitative analysis in tumor at different times (N=3). (C) Fluorescent quantitative analysis of ex vivo tumor and major organs at 6 d (N = 3). (D) CPT accumulation in tumors at day 3 and day 6 after tumor-bearing mice are injected with CPT-LFPR, CPT-LGPR and CPT at day 1 and day 4, expressed as injected dose per gram of tissue (% ID/g) (N = 3). (E) Tumor volume changes of mice treated with PBS, LFPR, CPT, CPT-LGPR and CPT-LFPR (N = 5). *p <0.05, **p <0.01 and ***p <0.001.

Quantitatively, for CPT-LFPR treated group, the average fluorescence intensity in tumor at day 4 and day 6 are 1.3-fold and 2.3-fold higher than that at day 1 and day 3, respectively (Figure 7B), which demonstrates the fibers preformed after the first i.v. injection can facilitate the accumulation of following i.v. injected CPT-LFPR. Finally, the mice are sacrificed at day 6, and the *ex vivo* fluorescence intensity of CPT-LFPR treated tumor is about 3.9-fold higher than CPT-LGPR group (Figure 7C and S26), which is in accordance with the quantitative result of CPT in tumor[39] (Figure S27), suggesting the tumor-specific cumulative effect of CPT-LFPR. For further precisely analyzing the cumulative effect of multiple administration, CPT-LFPR, CPT-LGPR or free CPT are i.v. injected into HeLa tumor-bearing mice with the same protocol as above mentioned and the three groups of mice are sacrificed at day 3 and day 6. The tumors are collected for determining the CPT concentration by homogenization and fluorescence measurement.[40] As shown in Figure 7D, for free CPT, CPT- LGPR and CPT-LFPR groups, the CPT accumulation in tumor at day 3 is 0.88%, 1.89% and 2.68% ID/g, respectively, where the highest CPT accumulation is detected in CPT-LFPR treated tumor. Moreover, at day 6, the CPT accumulation in the three groups is 0.89%, 1.96% and 6.30%, respectively. Compared with day 3, two control groups of free CPT and CPT-LGPR show little change at day 6. While the tumor accumulation in CPT-LFPR group at day 6 is 2.4-fold higher than that at day 3, which is in accordance with fluorescent quantification results *in vivo*. Furthermore, the fibrous structure can be observed by bio-TEM in tumor slices of CPT-LFPR treated mice, while not for PBS and CPT-LGPR groups (Figure S28). Therefore, the in situ formation of nanofibers and subsequent autocatalytic growth cause the effective accumulation of prodrugs, which may affect tumor growth *in vivo*.

The *in vivo* anti-tumor efficacy of peptide LFPR, free CPT, CPT-LGPR and CPT-LFPR is studied using HeLa tumor bearing BALB/c nude female mice. CPT-LFPR exhibits more significant tumor inhibition efficacy than other groups, which can be attributed to the enhanced prodrug accumulation in tumor site through autocatalytic morphology transformation (Figure 7E and S29). During the treatment, there are no obvious body weight losses for all mice groups (Figure S30), and the H&E staining shows no apparent organ damage (Figure S31).

CONCLUSION

In conclusion, an autocatalytic growth strategy is first introduced into drug delivery system for targeted drug accumulation *in vivo*. Considering slow nucleating and rapid growth process of nucleation based self-assembly, the "seed" can accelerate the formation of bulky nanoassembly via skipping the nucleating process, which is called an autocatalytic assembly. Through analysis of assembly kinetics of peptide-based prodrug CPT-LFPR in the presence of CtsB, the rate constant of autocatalytic assembly is obviously higher than that of nucleation based self-assembly. CPT-LFPR can instantly transform from nanoparticles to nanofibers with the assistance of preformed fibrils in tumor sites, which significantly improve the drug accumulation efficacy. Compared with the first i.v. injection, the second i.v. injection of CPT-LFPR exhibits up to 2.4-fold drug accumulation in tumor, implying improved cumulative effect of nanodrugs through multiple administrations. This drug delivery system based on autocatalytic self-assembly can suppress tumor growth effectively. Furthermore, by introducing various imaging agents and drugs into the autocatalytic morphology transformation platform, we can realize improved imaging and therapeutic efficacy of serious diseases.

ASSOCIATED CONTENT

Supporting Information

Experimental details, ^{1}H NMR, MALDI-TOF, WAXS, CD, FTIR, CLSM, TEM, as well as the data *in vitro* and *in vivo*. This material is available free of charge via the Internet at http://pubs.acs.org.

AUTHOR INFORMATION

Corresponding Author

E-mail: wanghao@nanoctr.cn (H. W.), qiaozy@nanoctr.cn (Z. Y. Q.)

Notes

The authors declare no competing financial interests.

ACKNOWLEDGMENT

This work was supported by National Natural Science Foundation of China (21704020, 21374026, 31870998, 51573032 and 51725302). China Postdoctoral Science Foundation (2017M620707).

REFERENCES

(1) Blanco, E.; Shen, H.; Ferrari, M. Principles of nanoparticle design for overcoming biological barriers to drug delivery. *Nat. Biotechnol.* **2015**, 33, 941.

(2) Deng, W.; Chen, W.; Clement, S.; Guller, A.; Zhao, Z.; Engel, A.; Goldys, E. M. Controlled gene and drug release from a liposomal delivery platform triggered by X-ray radiation. *Nat. Commun.* **2018**, 9, 2713.

(3) Dewhirst, M. W.; Secomb, T. W. Transport of drugs from blood vessels to tumour tissue. *Nat. Rev. Cancer* **2017**, 17, 738.

(4) Wilhelm, S.; Tavares, A. J.; Dai, Q.; Ohta, S.; Audet, J.; Dvorak, H. F.; Chan, W. C. W. Analysis of nanoparticle delivery to tumours. *Nat. Rev. Mater.* **2016**, 1, 16014.

(5) Sun, Q.; Zhou, Z.; Qiu, N.; Shen, Y. Rational design of cancer nanomedicine: nanoproperty integration and synchronization. *Adv. Mater.* **2017**, 29, 1606628.

(6) Overchuk, M.; Zheng, G. Overcoming obstacles in the tumor microenvironment: recent advancements in nanoparticle delivery for cancer theranostics. *Biomaterials* **2018**, 156, 217.

(7) Matsumoto, Y.; Nichols, J. W.; Toh, K.; Nomoto, T.; Cabral, H.; Miura, Y.; Christie, R. J.; Yamada, N.; Ogura, T.; Kano, M. R.; Matsumura, Y.; Nishiyama, N.; Yamasoba, T.; Bae, Y. H.; Kataoka, K. Vascular bursts enhance permeability of tumour blood vessels and improve nanoparticle delivery. *Nat. Nanotech.* **2016**, 11, 533.

(8) Liu, X.; Chen, Y.; Li, H.; Huang, N.; Jin, Q.; Ren, K.; Ji, J. Enhanced retention and cellular uptake of nanoparticles in tumors by controlling their aggregation behavior. *ACS nano* **2013**, 7, 6244.

(9) Li, L. L.; Qiao, S. L.; Liu, W. J.; Ma, Y.; Wan, D.; Pan, J.; Wang, H. Intracellular construction of topology-controlled polypeptide nanostructures with diverse biological functions. *Nat. Comm.* **2017**, 8, 1276.

(10) Yang, P. P.; Luo, Q.; Qi, G. B.; Gao, Y. J.; Li, B. N.; Zhang, J. P.; Wang, L.; Wang, H. Host materials transformable in tumor microenvironment for homing theranostics. *Adv. Mater.* **2017**, 29, 1605869.

(11) Qi, G. B.; Zhang, D.; Liu, F. H.; Qiao, Z. Y.; Wang, H. An "on-site transformation" strategy for treatment of bacterial infection. *Adv. Mater.* **2017**, 29, 1703461.

(12) Gao, Y.; Kuang, Y.; Guo, Z. F.; Guo, Z.; Krauss, I. J.; Xu, B. Enzyme-instructed molecular self-assembly confers nanofibers and a supramolecular hydrogel of taxol derivative. *J. Am. Chem. Soc.* **2009**, 131, 13576.

(13) Cai, Y.; Shen, H.; Zhan, J.; Lin, M.; Dai, L.; Ren, C.; Yang, S.; Liu, J.; Gao, J.; Yang, Z. Supramolecular "trojan horse" for nuclear delivery of dual anticancer drugs. *J. Am. Chem. Soc.* **2017**, 139, 2876.

(14) Huang, P.; Gao, Y.; Lin, J.; Hu, H.; Liao, H. S.; Yan, X.; Tang, Y.; Jin, A.; Song, J.; Niu, G.; Zhang, G.; Horkay, F.; Chen, X. Tumor-specific formation of enzyme-instructed supramolecular self-assemblies as cancer theranostics. *ACS nano* **2015**, 9, 9517.

(15) Yuan, Y.; Wang, L.; Du, W.; Ding, Z.; Zhang, J.; Han, T.; An, L.; Zhang, H.; Liang, G. Intracellular self-assembly of taxol nanoparticles for overcoming multidrug resistance. *Angew. Chem. Int. Ed.* **2015**, 54, 9700.

(16) Jonkheijm, P.; Schoot, P.; Schenning, A. P.; Meijer, E. W. Probing the solvent-assisted nucleation pathway in chemical self-assembly. *Science* **2006**, 313, 80.

(17) Tao, F.; Han, Q.; Liu, K.; Yang, P. Tuning crystallization pathways through the mesoscale assembly of biomacromolecular nanocrystals. *Angew. Chem. Int. Ed.* **2017**, 56, 1344.

(18) Niece, K. L.; Czeisler, C.; Sahini, V.; Tysseling-Mattiace, V.; Pashuck, E. T.; Kessler, J. A.; Stupp, S. L. Modification of gelation kinetics in bioactive peptide amphiphiles. *Biomaterials* **2008**, 29, 4501.

(19) Ban, T.; Yamaguchi, K.; Goto, Y. Direct observation of amyloid fibril growth, propagation, and adaptation. *Acc. Chem. Res.* **2006**, 39, 663.

(20) Jarrett, J. T.; Lansbury Jr, P. T. Amyloid fibril formation requires a chemically discriminating nucleation event: studies of an amyloidogenic sequence from the bacterial protein OsmB. *Biochemistry* **1992**, 31, 12345.

(21) Gulik-Krzywicki, T.; Fouquey, C.; Lehn, J. Electron microscopic study of supramolecular liquid crystalline polymers formed by molecular-recognition-directed self-assembly from complementary chiral components. *Proc. Natl. Acad. Sci. U. S. A* **1993**, 90, 163.

(22) Mason, T. O.; Michaels, T. C. T.; Levin, A.; Dobson, C. M.; Gazit, E.; Knowles, T. P.; Buell, A. K. Thermodynamics of Polypeptide Supramolecular Assembly in the Short-Chain Limit. *J. Am. Chem. Soc.* **2017**, 139, 16134.

(23) Baram, J.; Weissman, H.; Rybtchinski, B. Supramolecular polymer transformation: a kinetic study. *J. Phys. Chem. B* **2014**, 118, 12068.

(24) Kar, H.; Ghosh, G.; Ghosh, S. Solvent Geometry Regulated Cooperative Supramolecular Polymerization. *Chem. Eur. J.* **2017**, 23, 10536.

(25) Ai, X.; Ho, C. J. H.; Aw, J.; Attia, A. B. E., Mu, J., Wang, Y.; Wang, X.; Wang, Y.; Liu, X.; Chen, H.; Gao, M.; Chen, X.; Yeow, E. K. L.; Liu, G.; Olivo, M.; Xing, B. *In vivo* covalent cross-linking of photon-converted rare-earth nanostructures for tumour localization and theranostics. *Nat. Commun.* **2016**, 7, 10432.

(26) Kern, H. B.; Srinivasan, S.; Convertine, A. J.; Hockenbery, D.; Press, O. W.; Stayton, P. S. Enzyme-cleavable polymeric micelles for the intracellular delivery of proapoptotic peptides. *Mol. Pharmaceutics* **2017**, 14, 1450.

(27) Cheng, Y. J.; Luo, G. F.; Zhu, J. Y.; Xu, X. D.; Zeng, X.; Cheng, D. B.; Li, Y. M.; Wu, Y. Zhang, X. Z.; Zhuo, R. X.; He, F. Enzyme-induced and tumor-targeted drug delivery system based on multifunctional mesoporous silica nanoparticles. *ACS Appl. Mater. Interfaces* **2015**, 7, 9078.

(28) Biancalana, M.; Koide, S. Molecular mechanism of Thioflavin-T binding to amyloid fibrils. *Biochim. Biophys. Acta, Proteins Proteomics* **2010**, 1804, 1405.

(29) San, B. H.; Hwang, J.; Sampath, S.; Li, Y.; Bennink, L. L.; Yu, S. M. Self-Assembled Water-Soluble Nanofibers Displaying Collagen Hybridizing Peptides. *J. Am. Chem. Soc.* **2017**, 139, 16640.

(30) Lorenzen, N.; Nielsen, S. B.; Buell, A. K.; Kaspersen, J. D.; Arosio, P.; Vad, B. S.; Paslawski, W.; Christiansen, G.; Valnickova-Hansen, Z.; Andreasen, M.; Enghild, J. J.; Pedersen, J. S.; Dobson, C. M.; Knowles, T. P. J.; Otzen, D. E. The role of stable α-synuclein oligomers in the molecular events underlying amyloid formation. *J. Am. Chem. Soc.* **2014**, 136, 3859.

(31) Nichifor, M.; Schacht, E. H.; Seymour, L. W. Polymeric prodrugs of 5-fluorouracil. *J. Control. Release* **1997**, 48, 165.

(32) Tatai, L.; Moore, T. G.; Adhikari, R.; Malherbe, F.; Jayasekara, R.; Griffiths, I.; Gunatillake, P. A. Thermoplastic biodegradable polyurethanes: the effect of chain extender structure on properties and *in-vitro* degradation. *Biomaterials* **2007**, 28, 5407.

(33) Gilroy, J. B.; Gadt, T.; Whittell, G. R.; Chabanne, L.; Mitchels, J. M.; Richardson, R. M.; Winnik, M. A.; Manners, I. Monodisperse cylindrical micelles by crystallization-driven living self-assembly. *Nat. Chem.* **2010**, 2, 566.

(34) Nazemi, A.; Boott, C. E.; Lunn, D. J.; Gwyther, J.; Hayward, D. W.; Richardson, R. M.; Winnik, M. A.; Manners, I. Monodisperse cylindrical micelles and block comicelles of controlled length in aqueous media. *J. Am. Chem. Soc.* **2016**, 138, 4484.

(35) Humenik, M.; Magdeburg, M.; Scheibel, T. Influence of repeat numbers on self-assembly rates of repetitive recombinant spider silk proteins. *J. Struct. Boil.* **2014**, 186, 431.

(36) Morris, A. M.; Watzky, M. A.; Agar, J. N.; Finke, R. G. Fitting neurological protein aggregation kinetic data via a 2-step, minimal/"Ockham's Razor" model: The Finke-Watzky mechanism of nucleation followed by autocatalytic surface growth. *Biochemistry* **2008**, 47, 2413.

(37) Cheng, D. B.; Qi, G. B.; Wang, J. Q.; Cong, Y.; Liu, F. H.; Qiao, Z. Y.; Wang H. In Situ Monitoring Intracellular Structural Change of Nanovehicles through Photoacoustic Signals Based on Phenylboronate-Linked RGD-Dextran/Purpurin 18 Conjugates. *Biomacromolecules* **2017**, 18, 1249.

(38) Mold, M.; Kumar, M.; Mirze, A.; Shardlow, E.; Exley, C. Intracellular tracing of amyloid vaccines through direct fluorescent labelling. *Sci. Rep.* **2018**, 8, 2437.

(39) Zhu, Y.; Zhang, J.; Meng, F.; Deng, C.; Cheng, R.; Feijen, J.; Zhong, Z. cRGD-functionalized reduction-sensitive shell-sheddable biodegradable micelles mediate enhanced doxorubicin delivery to human glioma xenografts *in vivo*. *J. Control. Release* **2016**, 233, 29.

(40) Peng, Y.; Zhao, Z.; Liu, T.; Li, X.; Hu, X.; Wei, X.; Zhang, X.; Tan, W. Smart human-serum-albumin-As_2O_3 nanodrug with self-amplified folate receptor-targeting ability for chronic myeloid leukemia treatment. *Angew. Chem. Int. Ed.* **2017**, 129, 10985.

SYNOPSIS TOC